

Hydrogen Surface Reactions and Adsorption Studied on Y_2O_3 , YSZ, and ZrO_2

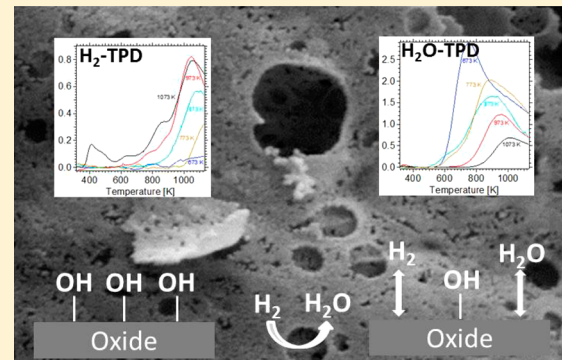
Michaela Kogler,^{†,‡} Eva-Maria Köck,^{†,‡} Thomas Bielz,[†] Kristian Pfaller,[‡] Bernhard Klötzer,[†] Daniela Schmidmair,[§] Lukas Perfler,[§] and Simon Penner*,[†]

[†]Institute of Physical Chemistry, University of Innsbruck, Innrain 52a, A-6020 Innsbruck, Austria

[‡]Section of Histology and Embryology, Medical University Innsbruck, Müllerstrasse 59, A-6020 Innsbruck, Austria

[§]Institute of Mineralogy and Petrography, University of Innsbruck, Innrain 52d, A-6020 Innsbruck, Austria

ABSTRACT: The surface reactivity of Y_2O_3 , YSZ, and ZrO_2 polycrystalline powder samples toward H_2 has been comparatively studied by a pool of complementary experimental techniques, comprising volumetric methods (temperature-programmed volumetric adsorption/oxidation and thermal desorption spectrometry), spectroscopic techniques (in situ electric impedance and in situ Fourier-transform infrared spectroscopy), and eventually structural characterization methods (X-ray diffraction and scanning electron microscopy). Reduction has been observed on all three oxides to most likely follow a surface or near-surface-limited mechanism involving removal of surface OH-groups and associated formation of water without formation of a significant number of anionic oxygen vacancies. Partly reversible adsorption of H_2 was proven on the basis of molecular H_2 desorption. Dictated by the specific hydrophilicity of the oxide, readsorption of water eventually takes place. The inference of this surface-restricted mechanism is further corroborated by the fact that no bulk structural and/or morphological changes were observed upon reduction even at the highest reduction temperatures (1173 K). We anticipate relevant implications for the use of especially YSZ in fuel cell research, since in particular the chemical state and structure of the surface under typical reducing high-temperature conditions affects the operation of the entire cell.



1. INTRODUCTION

The reducibility of oxides is one of the most important parameters determining their physicochemical characteristics, including structural, mechanical, electric, or catalytic properties. In essence, this is mostly affiliated with their defect chemistry. Focusing on the reducibility by hydrogen, both the formation and reactivity of hydrogen adsorbed on the oxide's surface are equally important in steering especially the catalytic properties of the respective oxide. This is related to both scenarios, where hydrogen takes part as an active component in the catalytic reaction (e.g., in the water–gas shift reaction) or simply creates defect or vacancy centers which subsequently serve as potentially active catalytic sites. Since Y_2O_3 , ZrO_2 , and especially YSZ (yttria-stabilized zirconia) are of widespread technological importance and are used as high-temperature-stable ceramics, protective toughening agents, or supporting oxides of heterogeneous catalysts (e.g., CO oxidation or hydrogenation, oxidation of hydrocarbons, or methanol conversion) equally,^{1–9} thorough understanding of the hydrogen chemistry especially at high temperatures is imperative. In comparison to Y_2O_3 and YSZ, despite the particular importance of the latter as an efficient ion conductor in solid-oxide fuel cells,⁶ ZrO_2 represents the best-studied oxide with respect to high-temperature treatments in hydrogen.^{10–12} It is considered a relatively inert oxide, notwithstanding considerable reduction

down to metallic Zr in hydrogen at temperatures at and above 1773 K.¹⁰ Nevertheless, ZrO_2 is capable of forming a range of substoichiometric oxides ZrO_{2-x} (thereby representing defective ZrO_2), which are suspected on the one hand to aid the catalytic decomposition of nitrous oxide¹³ or the synthesis of dimethyl carbonate from methanol and carbon dioxide¹⁴ and on the other hand to assist also the graphitization of carbon and the formation of carbon nanotubes.⁷ As pure ZrO_2 , after appropriate preparation and activation, is an effective catalyst for selective hydrogenation reactions, e.g., of CO toward ethanol or isobutanol in the temperature range between 600 and 700 K, a low-temperature surface H_2 reactivity of suitably prepared ZrO_2 samples should in principle be observable.¹⁵ With respect to ZrO_2 -supported catalyst systems, a range of metal particles (e.g., Ni, Rh, Cu, Pd, or Pt) supported on ZrO_2 were found to become promoted with respect to catalytic activity and selectivity, in particular after a high-temperature reductive treatment.^{8,15} This, in turn, raises important questions about the catalytic role of the purely oxidic surface itself and the prevalence of metal–support interaction effects especially in metal– ZrO_2 systems.⁸

Received: January 24, 2014

Revised: April 1, 2014

Published: April 2, 2014

Hydrogen reduction studies of pure Y_2O_3 and YSZ¹⁶ are scarce, which represents a considerable deficiency especially regarding the latter, since its technological application as anode/cermet material in solid-oxide fuel cells heavily depends on the nonstoichiometric behavior at elevated temperatures ($T \sim 1200$ K).

In the following we aim at providing a thorough comparative experimental study on the reducibility of the three aforementioned oxides in hydrogen to determine if, to what extent, and how H_2 -induced reduction of any of these oxides takes place. This will include the use of complementary methods to structurally and spectroscopically determine the presence of substoichiometric oxides (X-ray diffraction and FT-IR spectroscopy), to monitor changes in the electric properties during reduction (electrochemical impedance spectroscopy), and to qualitatively and quantitatively determine the extent of hydrogen adsorption and/or formation of oxygen defects/vacancies (temperature-programmed reduction and oxidation, thermal desorption). Special emphasis will also be given to the influence of the initial hydroxylation degree of the surface on the reducibility. The latter is considered particularly important, since related experiments on the adsorption of similar small probe molecules (CO and CO_2) not only showed a different degree of surface hydroxylation for the three oxides but also revealed the associated striking differences in adsorption capability.¹⁷ The final goal therefore is to determine if any substantial H_2 -induced reduction takes place at technologically relevant temperatures and how this might affect the technological applications.

2. EXPERIMENTAL SECTION

2.1. Materials. All experiments were conducted using commercially available powders of Y_2O_3 , ZrO_2 , and YSZ. Y_2O_3 (nanopowder with bcc structure, <50 nm particle size) and YSZ (yttria-stabilized zirconium(IV)oxide with tetragonal structure as nanopowder, containing 8 mol % Y_2O_3 as stabilizer, "YSZ-8") were obtained from Sigma-Aldrich and ZrO_2 (monoclinic, 99.978%) from Alfa Aesar. To ensure identical starting conditions, all samples were pretreated by calcination at 1173 K in air. Routine checking for structural changes by XRD upon annealing revealed no alterations (cf. Figure 8 below). After pretreatment, specific surface areas were determined as $21.7 \text{ m}^2 \text{ g}^{-1}$ (Y_2O_3), $31.6 \text{ m}^2 \text{ g}^{-1}$ (YSZ-8), and $10.4 \text{ m}^2 \text{ g}^{-1}$ (ZrO_2) by N_2 adsorption at 77 K using the BET method. For the BET measurements, a Quantachrome Nova 2000 Surface Area and Pore Size Analyzer was used. Gases were supplied by Messer (H_2 5.0).

2.2. FT-IR Spectroscopy. The FT-IR measurements were performed on a PerkinElmer FT-IR System 2000 Spectrometer in transmission mode. All powder samples were pressed into round pellets (sample mass about 100 mg each), which were subsequently placed inside a home-built *in situ* reaction cell. The path length of the IR reactor cell amounts to 20 cm. This cell setup allows treatments under both static and flowing conditions up to pressures of 1 bar and temperatures up to 873 K (for the work presented herein, experiments were only conducted under flowing conditions). The temperature is controlled by a thermocouple placed next to the pellet. After the pretreatment at 1173 K as mentioned above, the pellet was immediately transferred to the IR cell. Vacuum was applied subsequently (base pressure of the reaction cell: 10^{-6} mbar). Calcium fluoride is used as window material allowing to access wavelength ranges above 1000 cm^{-1} . To ensure identical

starting conditions, Y_2O_3 , ZrO_2 , and YSZ were oxidized with 20% oxygen seeded in helium at 873 K for 1 h inside the IR cell. To minimize the hydroxylation of the surface, all gases are cleaned and dried using two liquid nitrogen (reduction by H_2) or liquid nitrogen/ethanol cooling traps (reoxidation with O_2). All reported spectra are corrected by the spectrum of the dry preoxidized oxide pellet prior to hydrogen adsorption, in order to visualize changes relative to the initial fully oxidized state with a minimized degree of hydroxylation.

2.3. Volumetric Adsorption. The volumetric adsorption measurements were conducted in an all-quartz apparatus equipped with metal bellows valves (Witeg), a Baratron pressure transducer (MKS), mass flow controllers (MKS), and a Balzers QMA125 quadrupole mass analyzer. The furnace was a Linn model operating up to 1500 K. The previously fully oxidized samples (flowing oxygen up to 1273 K) were treated for 1 h in 1 bar flowing dry H_2 at a typical flow rate of 1 mL s^{-1} at different temperatures (373–1073 K). After this procedure, the sample was evacuated at room temperature to a base pressure of about 5×10^{-7} mbar and heated in high vacuum to 1273 K at a rate of 10 K min^{-1} (TPD measurements), followed by cooling in vacuum to room temperature. The subsequent temperature-programmed oxidation (TPO) measurements up to 1273 K, performed under static O_2 conditions, allowed us to study the reoxidation process and the amount of oxygen required for complete reoxidation and quenching of reduced metal centers, although in the present case the exact quantitative determination is severely obscured by the variable hydroxylation degree of the surface. For the volumetric experiments, all mass spectrometer data (in mbar) were converted into μmol on the basis of the ideal gas equation, with subsequent normalization to sample mass and surface area. Cleaning of the gases is performed as mentioned in section 2.2.

2.4. X-ray Diffraction. X-ray powder diffraction data were collected at ambient conditions with a Bruker AXS D8 Discover high-resolution powder diffractometer using monochromatic $\text{Cu}-\text{K}_{\alpha 1}$ radiation ($\lambda = 1.5406 \text{ \AA}$; 40 kV, 40 mA) and a one-dimensional LynxEye detector. The monochromatization of the Cu radiation was ensured by a presample Quartz (101) beam monochromator. Data acquisition was performed in the 2θ range between 2 and 80° using a step width of 0.011° and a counting time of 3 s. To avoid misinterpretation of the measured intensity, a fixed divergence slit (opening angle of 0.3°) was used.

2.5. Electrochemical Impedance Measurements. The impedance cell is suited for gas treatments compatible with those in the volumetric and FT-IR measurements. Heating was performed by a tubular furnace and is controlled by a thermocouple situated in the reactor about 5 mm downstream of the sample and a Micromega PID temperature controller. The sample impedance was measured by an IM6e impedance spectrometer (Zahner-Elektrik), which supplied data on the impedance and the phase angle of the current as a function of voltage (20 mV) in a frequency range of 0.1–1 MHz. For all oxide measurements described herein, a very low excitation frequency of 1 Hz and a stimulation voltage of 20 mV applied to two circular Pt electrodes with a contact area of about 20 mm^2 forming a plate capacitor in a vertical quartz tube were used. A mechanical force of $\sim 2 \text{ N}$ thereby results.¹⁸ For a typical experiment, the samples were heated up to 1073 K, held at 1073 K for 30 min, and subsequently cooled down to 300 K at a rate of 10 K min^{-1} in the respective gas atmosphere under

flowing conditions ($\sim 0.9 \text{ mL s}^{-1}$). Cleaning of the gases is performed as mentioned in section 2.2.

2.6. Scanning Electron Microscopy. All SEM experiments were conducted using an SM 982 GEMINI ZEISS Field Emission Scanning Electron Microscope. Prior to SEM imaging, the samples were coated with 10 nm Au/Pd to improve its conductance and fixed with conducting carbon paste.

3. RESULTS AND DISCUSSION

3.1. Temperature-Programmed Reduction (TPR). All samples were heated under vacuum to 1273 K followed by full oxidation under flowing dry oxygen ($\text{N}_2/\text{ethanol}$ cooling trap, 173 K) up to 1273 K and back prior to the actual hydrogen measurement. After evacuating the system at 300 K to $< 10^{-6}$ mbar, the samples were exposed to an exactly measured pressure between 90 and 100 mbar of dry hydrogen (dosed via a LN_2 cooling trap), followed by a volumetric heating and cooling cycle between 300 and 1273 K in static H_2 conditions. A linear heating and cooling rate of 10 K min^{-1} was applied, as well as an isothermal period of 10 min at the maximum temperature. To determine the eventual influence of the hydroxylation degree of the oxide surfaces, similar experiments with and without a preinstalled and thoroughly dried/degassed zeolite trap, capable of removing water eventually being formed during the reaction with hydrogen, were performed.

Figure 1 illustrates the corresponding hydrogen uptake traces with the zeolite trap installed, which are not obscured by H_2O

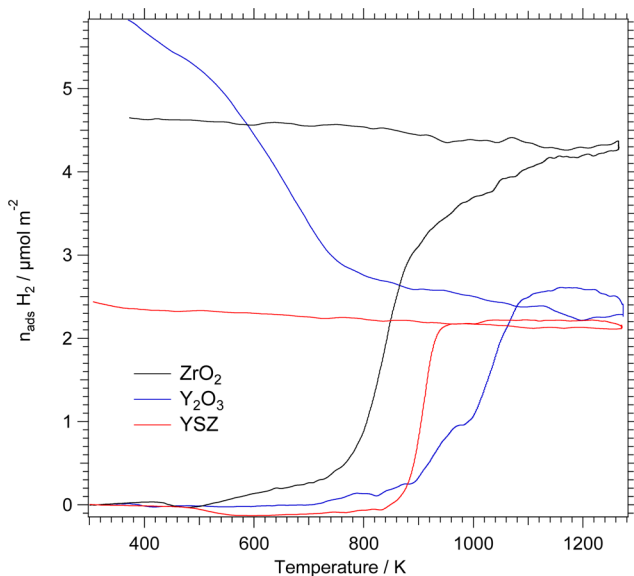


Figure 1. Volumetric hydrogen uptake during temperature-programmed reduction (TPR). A heating and cooling cycle between 300 and 1273 K for ZrO_2 (black trace), Y_2O_3 (blue trace), and YSZ (red trace) with a zeolite trap, installed in the cold part of the volumetric cell in close vicinity to the sample to remove the reaction-induced water, was performed.

formation due to surface reduction. For all studied systems, the qualitative behavior of hydrogen adsorption, at least upon heating, is the same. All samples show an induction period without pronounced hydrogen adsorption (ZrO_2 up to 500 K, Y_2O_3 up to 700 K, YSZ up to 820 K). Above these temperatures, significant hydrogen adsorption and uptake is observed on all three studied systems, which exhibit one or

more significantly discernible hydrogen-consuming adsorption or reaction steps. For ZrO_2 , two steps of hydrogen uptake ($\sim 500 \text{ K} - 0.5 \mu\text{mol m}^{-2}$; $\sim 800 \text{ K} - 4.3 \mu\text{mol m}^{-2}$) are observed. At the maximum temperature some isothermal uptake, remaining irreversible upon cooling ($\sim 4.6 \mu\text{mol m}^{-2}$), is visible. In contrast, for YSZ only one step in hydrogen uptake ($\sim 830 \text{ K} - 2.5 \mu\text{mol m}^{-2}$), which again is not reversible upon cooling, is observed. Almost no isothermal uptake takes place at 1260 K.

Y_2O_3 shows at least two distinct steps of hydrogen uptake and also no isothermal uptake at the maximum temperature. Nevertheless, in striking contrast to what was observed on the other two oxides, upon cooling below $\sim 750 \text{ K}$ a quite pronounced increase of the hydrogen uptake is visible, indicating that during the preceding high-temperature reduction some low-temperature hydrogen adsorption sites are formed (compare the corresponding TPD spectra shown in Figure 3, panel A for reduction temperatures $T \geq 973 \text{ K}$). This peculiar feature is focused upon in more detail in the discussion of Figure 2.

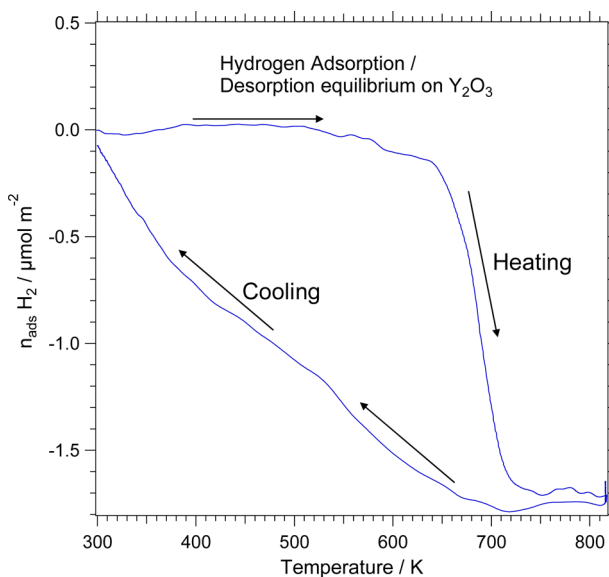


Figure 2. Heating–cooling cycle (between 300 and 800 K) starting again from 90 to 100 mbar static H_2 atmosphere on the Y_2O_3 sample following temperature-programmed reduction up to 1273 K. Linear heating and cooling rate: 10 K min^{-1} .

In general, ZrO_2 is somewhat more prone to react with hydrogen already at lower temperatures in comparison to Y_2O_3 and YSZ, which is further corroborated by the TPD measurements discussed in Figure 3. Putting all uptake values of this present comparison into perspective, we, however, note that for all three oxides the hydrogen uptake is still small compared to easy-reducible oxides. In_2O_3 , for example, shows a hydrogen uptake of about $13 \mu\text{mol m}^{-2}$ already at reduction temperatures of 673 K .¹⁹

Although discernible reduction steps cannot be resolved in the case of YSZ, both ZrO_2 and Y_2O_3 show clearly discernible plateaus (ZrO_2 between 450 and 750 K, Y_2O_3 between 700 and 800 K). Apparently, in the latter two cases, at least two kinetically different ways to bind hydrogen are present. The plateaus at lower reduction temperatures are clearly associated with predominant surface reduction associated with water formation. The steep increase of the H_2 -uptake step at higher

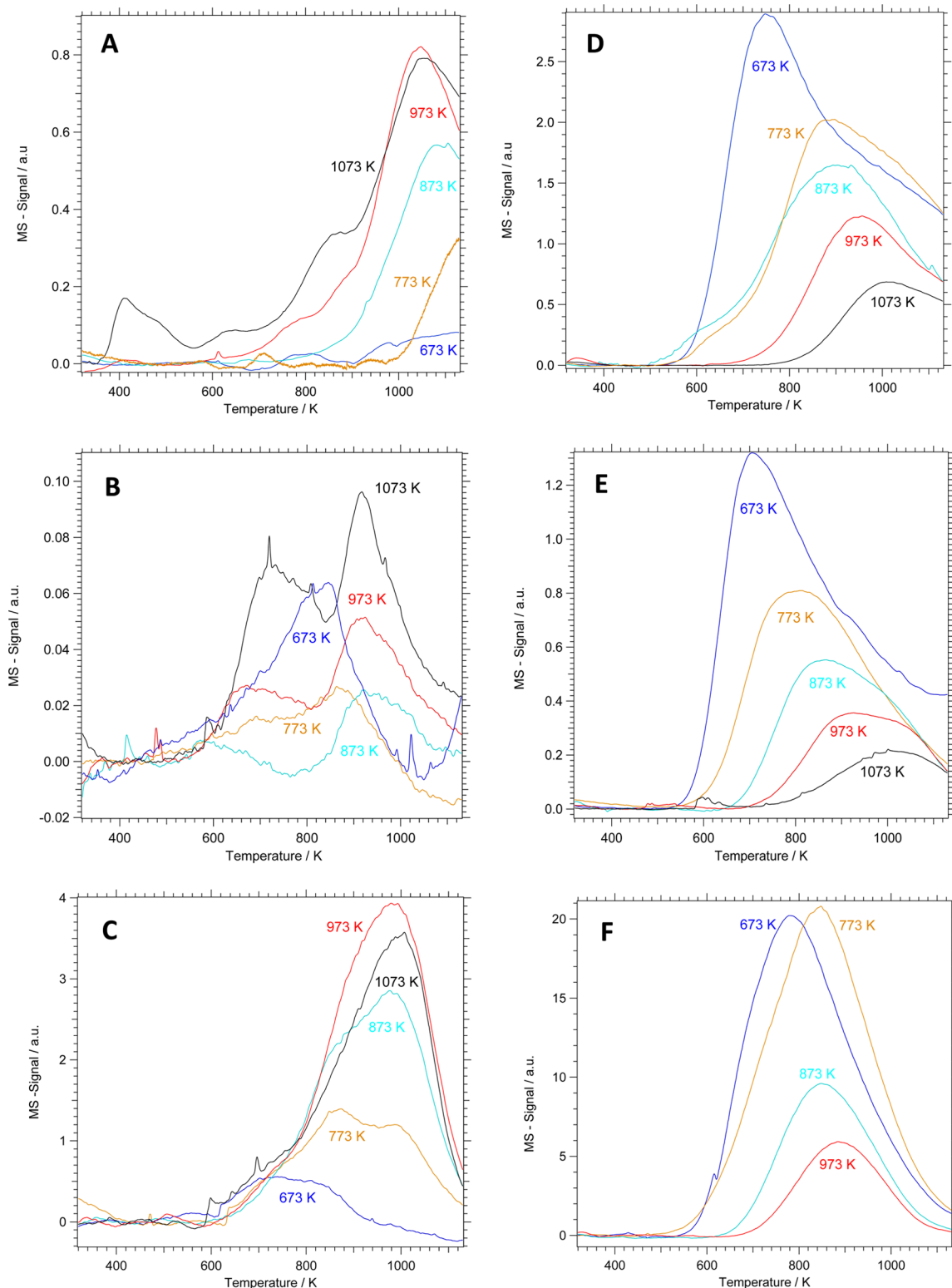


Figure 3. Temperature-programmed hydrogen and water desorption spectra as a function of prereduction temperature. The hydrogen desorption spectra are shown in panels A–C, the water desorption spectra in panels D–F: Y₂O₃ (upper panels A and D), YSZ (middle panels B and E), ZrO₂ (lower panels C and F). Linear heating rates of 10 K min⁻¹ were applied. The prereduction was carried out at each temperature for 1 h in 1 mL s⁻¹ flowing dry hydrogen (N₂ cooling trap). Note that although the unit of the MS signal is given in a.u., we chose to provide numbers for better internal comparison, since all TPD spectra were measured using the same detection sensitivity.

reduction temperatures might be associated with reduction of surface-near regions, whereas bulk reduction is not accessible in the studied temperature range (compare the XRD diffractograms in Figure 8 below). This is also reflected in the TPD

spectra discussed below, which especially at higher reduction temperatures clearly show combined desorption of hydrogen and/or water from chemically different adsorption or defect sites. The stagnation of hydrogen uptake at higher reduction

temperatures and the general absence of a pronounced isothermal hydrogen uptake at the highest reduction temperatures $T \geq 1000$ K point to a very slow, kinetically strongly hindered reduction process; i.e., the major part of the reducible sites is apparently consumed at this stage. Regarding the hydrogen uptake on ZrO_2 , our results are in line with those provided by Hoang et al., who observed some hydrogen uptake beginning at 823 K.⁸

Similar experiments have also been performed without zeolite trap, but these are severely obscured by H_2O -induced pressure effects, finally leading to uninterpretable results.

To shed more light on the pronounced and distinct hydrogen reuptake on Y_2O_3 upon cooling below ~ 700 K, which was only observed after a preceding high-temperature hydrogen treatment to 1273 K (Figure 1, Y_2O_3 cooling curve), Figure 2 shows an immediately following H_2 -TPR run only up to 800 K (after evacuation and redosing of again ~ 90 –100 mbar H_2). This experiment was performed as a test for potential reversibility of molecular H_2 adsorption on the high-temperature prereduced Y_2O_3 sample. Upon heating, hydrogen desorbs from the surface and is again readsorbed upon cooling. In this experiment, only the cooling curve perfectly fits to the analogous uptake observed during the cooling of Figure 1 (Y_2O_3). Interestingly, this partially reversible phenomenon appears to be significantly affected by kinetic limitations, as a pronounced hysteresis between heating (desorption) and cooling (readsorption) is observed. Nevertheless, quasi-equilibrium amounts of molecularly adsorbed H_2 can be established at 300 and 800 K, respectively.

As this phenomenon is only observed after high-temperature H_2 reduction, dedicated special sites for molecular H_2 adsorption are likely present at the surface. The kinetic hysteresis between 300 and ~ 730 K can be tentatively explained by a considerable kinetic desorption barrier for molecular H_2 , which is largely overcome at $T > 650$ K (steep drop at 630 K).

3.2. Temperature-Programmed Desorption. To analyze the formation of special hydrogen reduction-induced “molecular” hydrogen binding sites, temperature-programmed H_2 desorption runs following reduction at temperatures between 673 and 1073 K have been similarly performed on all samples. As for the technical details, again linear heating and cooling rates of 10 K min^{-1} were applied. Prereduction was carried out at each given temperature for 1 h in 1 mL s^{-1} flowing dry hydrogen (N_2 cooling trap). Figure 3 in turn gives a compact overview of both the hydrogen and water traces, observed after prereduction at the respective temperatures and subsequent desorption. Panels A and D show the experiments on Y_2O_3 , panels B and E those on YSZ, and panels C and F those on ZrO_2 . What immediately catches one’s attention is that generally all three samples show rather pronounced water desorption signals compared to the hydrogen desorption signals after low prereduction temperatures. With increasing prereduction temperature, the water signals decrease in relative intensity and the molecular hydrogen signals correspondingly become predominant. Above 973 K prereduction temperature, Y_2O_3 shows additional low-temperature hydrogen desorption states (~ 800 and ~ 400 K), getting more pronounced at 1073 K prereduction temperature. Most importantly, after reduction at 1073 K, even more low-temperature desorption states are present (at ~ 420 , ~ 620 , ~ 840 K), which perfectly fits to the quasi-reversible molecular H_2 -uptake during cooling as shown in the TPR measurements (cf. Figures 1 and 2). The low-

temperature desorption states up to 600 K are exclusively present on Y_2O_3 , which again corroborates the H_2 results of the TPR experiments. For YSZ, panel B reveals a single desorption peak at ~ 800 K after prereduction at 673 K with a low-temperature shoulder at ~ 700 K. This shoulder gets more pronounced, especially at prereduction temperatures of 773, 973, and 1073 K, indicating the presence of at least two different binding sites for hydrogen. The associated water signals follow exactly the same trend as for Y_2O_3 , with the water signals gradually decreasing upon increasing the prereduction temperature and the desorption maximum shifting to higher temperatures. Note, however, that the associated hydrogen binding sites on Y_2O_3 and YSZ appear to be different, as the qualitative shape of the TPD trace is clearly different. The hydrogen desorption spectra on ZrO_2 reveal a single broad feature with two peaks at low prereduction temperatures (~ 700 and ~ 800 K), with a high-temperature shoulder at ~ 1000 K, getting progressively the dominant feature at higher prereduction temperatures. The water traces on ZrO_2 do not show a clear trend, although for 673, 873, and 973 K, at least the intensity trend does indeed resemble those observed on Y_2O_3 and YSZ. The temperature maxima and the relative fraction of H_2 and H_2O normalized to the total TPD intensity are summarized for the lowest and the highest prereduction temperature in Table 1.

Table 1. Temperature Maxima of the H_2 - and H_2O -TPD Peaks alongside Relative Fraction of H_2 and H_2O Normalized to the Total TPD Intensity for Different Prereduction Temperatures

	Y_2O_3 673 K	YSZ 673 K	ZrO_2 673 K
H_2	$T > 1140$ K 2%	$T \sim 840$ K 4%	$T \sim 740$ K 2%
H_2O	$T \sim 720$ K 98%	$T \sim 700$ K 96%	$T \sim 760$ K 98%
	Y_2O_3 973 K	YSZ 973 K	ZrO_2 973 K
H_2	$T \sim 1040$ K 36%	$T \sim 920$ K 13%	$T \sim 960$ K 44%
H_2O	$T \sim 940$ K 64%	$T \sim 920$ K 87%	$T \sim 880$ K 56%

3.2. FT-IR Spectroscopy. To follow hydrogen reactivity spectroscopically and to detect the temperature-dependent degree of hydroxylation of the respective surface, FT-IR spectroscopic measurements have been performed on all three oxides in H_2 atmosphere. Figure 4 highlights temperature-dependent experiments following a heating–cooling cycle in streaming hydrogen (1 mL s^{-1}), in close correlation to the temperature-programmed reduction studies discussed in Figure 1. Note that, due to the limited temperature range available in the *in situ* FT-IR cell, only the onset of hydrogen reactivity could be studied. What immediately catches one’s attention is that upon heating in hydrogen, gaseous water is formed on all three oxides, beginning at 573 K and further increasing with increasing reduction temperature. With respect to Y_2O_3 , two negative peaks appear at 3706 and 3675 cm^{-1} upon heating. As negative peaks indicate vanishing of a formerly present hydroxyl species, we address these peaks to reactive, possibly isolated, OH-groups, which appear to be only weakly associated with other OH-groups on the surface and are therefore rather reactive. Even at room temperature, removal of these species already starts. These isolated hydroxyl species have been discussed in a previous publication in terms of their influence on CO and CO_2 adsorption¹⁷ and are a commonly discussed feature in oxide surface chemistry, e.g., on HfO_2 ,²⁰ SnO_2 ,²¹ (termed “terminal” OH-groups), or ZrO_2 .²² The signals of

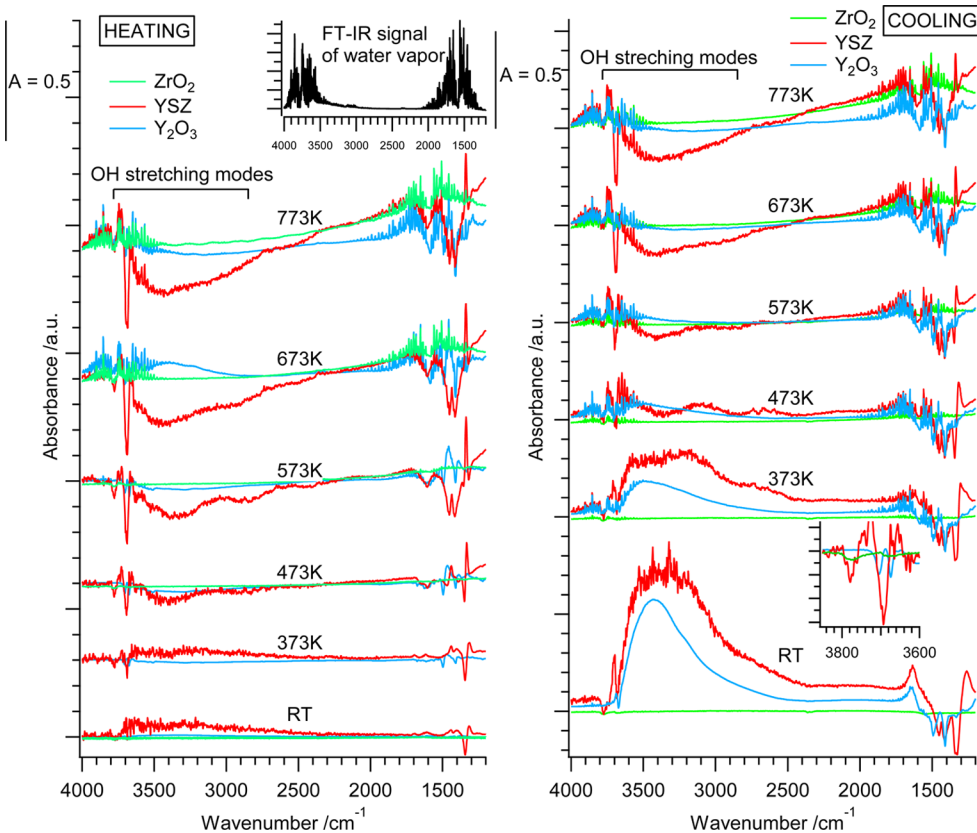


Figure 4. Temperature-dependent FT-IR spectra taken in flowing hydrogen (1 mL s^{-1}) on Y_2O_3 (blue trace), YSZ (red trace), and ZrO_2 (green trace) following a heating cycle from room temperature (300 K) to 773 K (panel A) and back to 300 K (panel B). The inset in panel A shows the FT-IR spectrum of water vapor, the inset in panel B the OH-region of the heating cycle at 473 K. Important peak regions have been marked.

stretching vibrations of these predominantly low-coordinated OH-groups are accordingly shifted to higher wave numbers in comparison to those connected via additional hydrogen bonds.²² The metal–O bond therefore is strongest, accordingly weakening the corresponding O–H bond. Stepwise cooling (panel B) yields a gas-phase water spectral signature of Y_2O_3 , and a broad “associated” OH peak is obtained. The dehydroxylation trends of YSZ resemble those seen on Y_2O_3 upon annealing in hydrogen. The two peaks of the isolated OH groups are found at 3777 and 3694 cm^{-1} (cf. inset in panel B). Nevertheless, the presence of possible dimer OH groups, usually observed at lower wave numbers, is higher. Assuming neighboring Y^{3+} and Zr^{4+} centers in YSZ, formation of specific dimers on such centers is plausible (potential formation of a $\text{Zr}^{4+}\text{--Y}^{3+}\text{--}(\text{OH})_2$ pair). On ZrO_2 , only two very weak OH signals, very much coinciding with those of YSZ, are obtained. ZrO_2 appears to be largely inert toward water and the gas-phase water species is predominant, which is increasingly formed at higher temperatures. Water readsorption is largely suppressed on ZrO_2 . In summary, the FT-IR experiments convincingly show that the reduction of the respective oxides in hydrogen in essence is connected with their surface water chemistry. Deeper reduction, including the formation of hydride phases, was not observed. Indirectly, we can conclude that molecular H_2 adsorption is linked to progressive H_2 -induced surface dehydroxylation, whereby dehydroxylated sites at originally “isolated” OH-groups are formed kinetically more easily.

3.3. Electrochemical Impedance Spectroscopy (EIS).

Alternating current (ac) impedance analysis was carried out for the Y_2O_3 , YSZ, and ZrO_2 samples to detect changes in the

conductivity, as well as eventual stoichiometry changes during treatment in hydrogen. Prior to every EIS measurement, the samples were heated in dry flowing O_2 ($\sim 0.3 \text{ mL s}^{-1}$) to 1273 K. After an isothermal period at 1273 K for 30 min, the samples were cooled to 300 K, again in O_2 . Arrhenius plots of $\ln(\text{conductivity})$ versus the inverse of the respective annealing temperature were subsequently used to calculate the apparent activation energies for charge transport for the different heating and cooling processes. Table 2 shows the values of these activation energies (E_A) for the experiments of the three samples using dry and moist hydrogen.

Table 2. Activation Energies for the Heating and Cooling Curves in Dry and Moist H_2 for All Three Oxides^a

	$E_A \text{ H}_2 \text{ dry}/\text{mol}^{-1} \text{ kJ}$	temp range/K	$E_A \text{ H}_2 \text{ moist}/\text{mol}^{-1} \text{ kJ}$	temp range/K
Y_2O_3 heating	87	557–824	73	603–825
Y_2O_3 cooling	64	555–833	49	612–825
YSZ heating	101	664–1068	102	646–1080
YSZ cooling	105	665–1078	104	646–1081
ZrO_2 heating	46	643–1043	40	644–994
ZrO_2 cooling	46	641–1071	43	641–950

^aThe temperature range indicates the temperature range with linear Arrhenius behavior used for calculation of E_A .

Exposure of the YSZ sample to dry hydrogen and heating to 1073 K shows an impedance decrease of about 5 orders of magnitude. The heating and cooling traces almost perfectly follow the same trend in the temperature range from 550 to 1073 K. Only below ~ 550 K, the heating curve exhibits a stronger temperature dependence than the respective cooling trace. As shown in Figure 5B, heating and cooling in moist

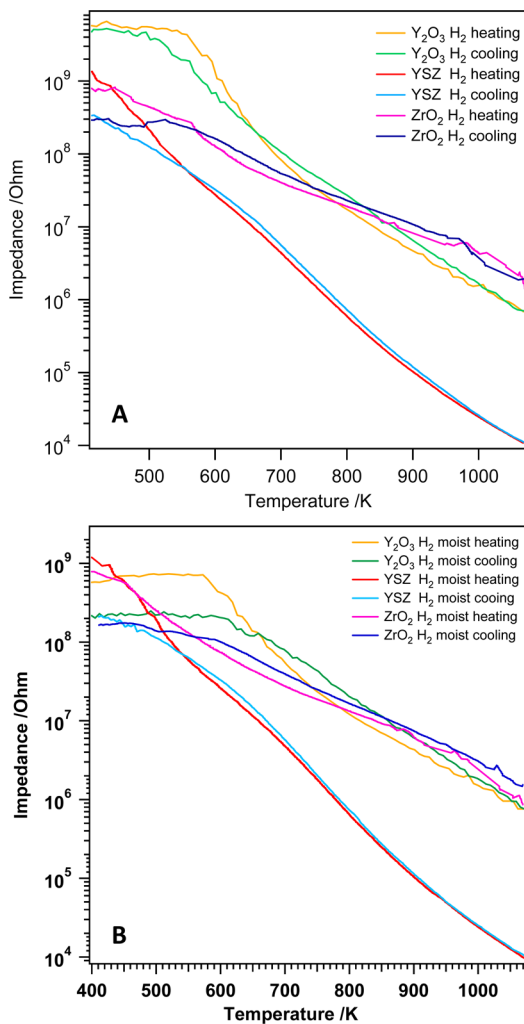


Figure 5. In-situ electric impedance spectra measured on Y₂O₃, YSZ, and ZrO₂ after a heating–cooling cycle in dry (panel A) and moist hydrogen (panel B) between 373 and 1073 K. Isothermal period at 1073 K for 30 min, heating and cooling rate: 10 K min⁻¹.

hydrogen show exactly the same behavior. Only if the sample was cooled down to room temperature in moist hydrogen, a very strong decrease of the impedance was observed experimentally (cf. Figure 6, impedance value prior to reoxidation in dry oxygen). According to a study by Scherrer et al.,²³ three temperature regions with different conduction mechanisms can be distinguished on YSZ: room temperature–400 K: proton conduction mediated by a physisorbed water layer (Grothus mechanism); 400–673 K: mixed conduction by oxygen ions as well as protons; above 673 K: pure oxygen ionic conductivity with an activation energy of ~ 100 kJ mol⁻¹. On this basis, we interpret the impedance increase between room temperature and 430 K in Figure 6 (heating curve) in terms of the desorption of a physisorbed water layer causing a high contribution of proton conduction. In the temperature range

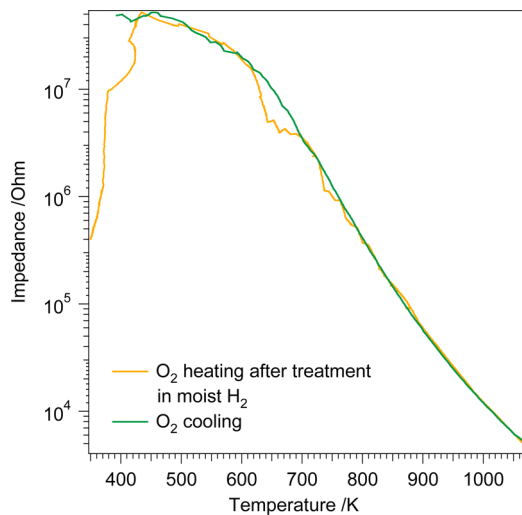


Figure 6. In-situ electric impedance spectra measured on YSZ after a heating–cooling cycle in moist hydrogen followed by a reoxidation treatment in dry oxygen (temperature ramp between 373 and 1073 K). Isothermal period at 1073 K for 30 min, heating and cooling rate: 10 K min⁻¹.

between 430 and 650 K, the decrease of impedance with temperature is less pronounced than above ~ 673 K (compare both with Figures 5 and 6) corresponding to the mixed hydroxyl–proton and oxide ion transport mechanism postulated by Scherrer et al. (variation of activation energy between ~ 50 and ~ 100 kJ mol⁻¹).²³ Beyond 673 K, the pure bulk oxide ion transport is prevalent (activation energy ~ 100 kJ mol⁻¹, cf. Table 2). The divergence of the heating and cooling curves in hydrogen below ~ 550 K (both Figure 5A and B) is not yet fully understood but may be due to an increased contribution of the hydroxyl-mediated proton transport after cooling in hydrogen, which may lead to increased hydroxylation of the sample surface. Thus, an overproportional contribution of the hydroxyl-mediated proton transport may result. This is corroborated by the FT-IR spectra shown in Figure 4, clearly showing an enhanced number of hydroxyl groups on the surface after cooling in hydrogen to room temperature.

The interpretation of the data on Y₂O₃ and ZrO₂ is unfortunately less straightforward; the only effect which can be safely assumed is a strongly reduced contribution of bulk oxide ion conductivity in both cases. Also the total number of available charge carriers is likely much lower than in the case of YSZ. As can be deduced from the data in Table 2, activation barriers for Y₂O₃ range from ~ 50 to 90 kJ mol⁻¹ in the temperature range 550–830 K, and for ZrO₂ even lower values of around 45 kJ mol⁻¹ were observed (~ 650 –1050 K). Regarding monoclinic ZrO₂, some data on the temperature-dependent impedance change upon treatment in hydrogen are available. Formation of surface and bulk oxygen vacancies has been observed below and above 873 K, accompanied by the release of electrons. Activation energies of ~ 25 and ~ 115 kJ mol⁻¹ for surface and bulk vacancy formation have been reported.²⁴ Unfortunately, the data are not related to the degree of surface hydroxylation. Nevertheless, the low apparent activation energy obtained in this work (~ 45 kJ mol⁻¹) clearly points to the prevalence of a surface-bound process, possibly also involving hydroxylated species. For hydrated ZrO₂ samples, nevertheless, a proton-based conductivity on the surface has also been inferred.²⁵ As the band gaps of

stoichiometric Y_2O_3 , YSZ, and ZrO_2 exhibit values of ~ 5.8 eV (580 kJ mol^{-1}),²⁶ ~ 5.9 eV (590 kJ mol^{-1}),²⁷ and ~ 6 eV (600 kJ mol^{-1}),²⁸ pure bulk electron excitation is excluded.

It is worth noting, that Y_2O_3 does not follow the trend of the apparent activation energies observed for both YSZ and ZrO_2 ; that is, similar activation energies are obtained no matter if the heating or cooling curves are used for evaluation. Rather, in the case of Y_2O_3 , the apparent activation energies are much lower in case the evaluation is solely based on the cooling curves. As the hydroxylation degree of Y_2O_3 is much higher compared to the other two oxides, we anticipate a strongly temperature-dependent coverage with adsorbed water during heating and cooling and correspondingly altered activation energies. A proton-mediated surface-bound conductivity mechanism is therefore highly likely, given the high hydroxylation degree. In due course, cooling in hydrogen leads to more effective rehydroxylation, a stronger contribution of this proton-mediated mechanism, and possibly also a smaller activation energy.

3.4. Structural Characterization. To obtain complementary information about the influence of the hydrogen treatment on the structure and morphology of the samples, scanning electron microscopic images and X-ray diffraction patterns have been additionally collected. Figure 7 summarizes the changes in particle and grain morphology and shows the respective oxides after the hydrogen treatment at 1173 K. In short, the morphology of all three oxides remains unaltered with respect to before the treatment. Exemplarily discussed for Y_2O_3 in panel A, the inset highlights the sample in the initial state. The untreated sample itself consists of small rounded grains of about 20 nm size, agglomerating to larger flakelike and splintered arrangements. Panel A correspondingly shows the morphology of the surface of one such grain after reduction at 1173 K. By comparison of the two images, it is immediately obvious that the grain size did not change and no sintering is observed; i.e. the porosity of the sample is unaffected by the treatment. Although the intrinsic morphology of YSZ (panel B, nanometer-sized three-dimensional grain aggregates) and ZrO_2 (panel C, well-faceted grains of about 100 nm size) is different, they are equally unaffected by the hydrogen treatment. As for the observations of eventual changes in the crystallographic structure of the samples upon reduction, XRD diffractograms equally reveal no substantial changes. Although it is known that ZrO_2 basically remains unaffected by reduction in hydrogen up to temperatures of 1773 K,⁸ it is worth noting that also Y_2O_3 and especially YSZ do not show signs of structural changes at typical operational conditions of, e.g., a solid oxide fuel cell.

3.5. Discussion. Taking the presented results together, a more detailed picture of the reduction mechanism, for all presented oxides, evolves. As structural (bulk) characterization methods show changes neither in the morphology nor in the structure of the samples upon reduction, we infer a mechanism that is restricted to the surface or at least surface-near regions. This is corroborated both by the fact that volumetric adsorption and thermal desorption techniques indeed show consumption/desorption of hydrogen and water by/from the surface and that electric impedance measurements do only show the reversible formation of thermally excited charge carriers, but not a substantial formation of thermally easily excitable donor electron states, e.g., at F-centers. Combination of these results with those from FT-IR spectroscopy reveals the crucial importance of the degree and nature of surface hydroxylation for hydrogen adsorption and reactivity. There

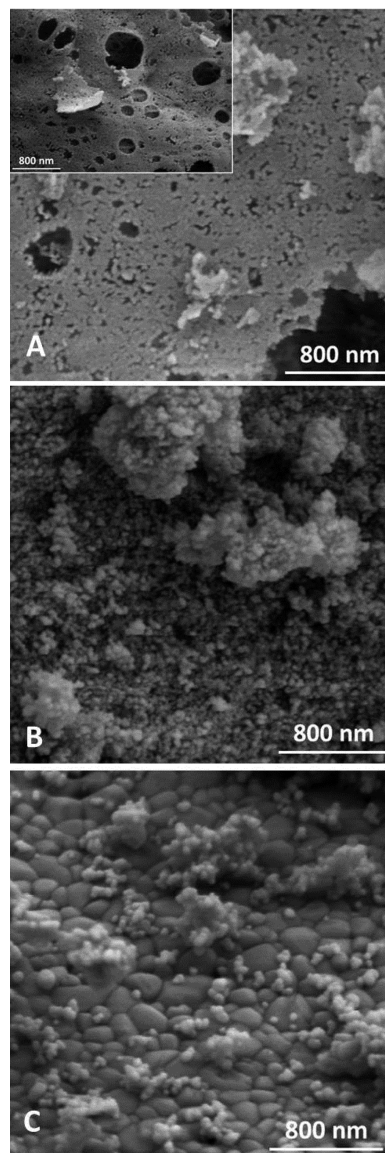


Figure 7. Scanning electron microscopic images taken after reduction of Y_2O_3 (panel A), YSZ (panel B), and ZrO_2 (panel C) in hydrogen at 1173 K. The inset in panel A highlights the initial Y_2O_3 sample before reduction.

is hard experimental evidence that the reduction of the oxides follows a mechanism where hydrogen adsorbs on the surface, reacting with OH-groups of the surface by forming water, which, depending on the hydrophilicity of the oxides, remains adsorbed or readsorbs on the surface at lower temperatures. Although unfortunately no corresponding literature data especially for Y_2O_3 exist, our results are in line with reports by Pomfret et al.¹³ on the existence of surface-stabilized low-valence metal states upon reduction of YSZ in hydrogen at 1273 K. The authors observed considerable changes neither in XRD patterns nor in Raman frequencies upon reduction but did observe a chemical reduction of the surface and surface-near regions of both yttrium and zirconium to lower valence states. These are also most likely responsible for the observed molecular H_2 adsorption effect. Unfortunately, no information on the hydroxylation degree of the YSZ surface is presented in the paper of Pomfret et al.,¹⁶ but results by Raz et al.²⁹ strongly indicate that adsorbed water facilitates the ionic conduction via

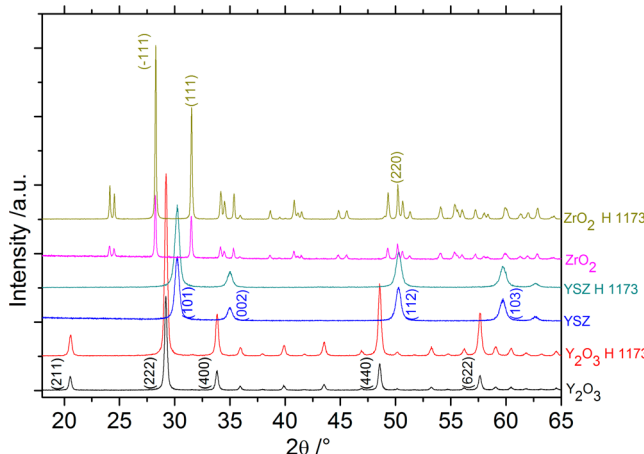


Figure 8. X-ray diffractograms of the initial Y_2O_3 , YSZ, and ZrO_2 samples and after reduction in hydrogen at 1173 K. Important reflections have been marked. “Initial” refers to the respective states after calcination in air at 1173 K before the actual reduction.

the aforementioned proton-based surface-bound mechanism. Given the clear coincidences of the results from all three oxides, we may safely assume that a corresponding near-surface-limited reduction prevails on Y_2O_3 , YSZ, and ZrO_2 . Differences only arise due to the different number of OH-groups present on the respective surfaces before reduction. As already previously reported, Y_2O_3 is the most hygroscopic of the three oxides.¹⁴ On the contrary, the corresponding number of OH-groups is lowest on ZrO_2 , at least on the sample that was used for the presented studies. Regarding the reduction of the latter, bulk reduction was clearly not anticipated in the present work, as it has been long known that even using atomic hydrogen, no substantial bulk reduction takes place.⁸ However, given the use of low-valent Zr compounds in catalysis and organic synthesis (e.g., decomposition of nitrous oxide,¹³ synthesis of dimethyl-carbonate from methanol and carbon dioxide¹⁴) and also the suspected activity of oxygen defects present in nanoparticulate ZrO_2 in carbon nanotube growth,⁷ we infer that the reduction of ZrO_2 and its ability to bind H_2 molecularly is restricted to the strongly reduced and dehydroxylated surface-near regions also in all the literature-discussed cases. A particular important topic regarding the presence of low-valent Zr compounds is related to metal–support interaction. Although still subject to discussion, there is also experimental evidence that ZrO_2 -supported metal catalysts become active after a treatment in hydrogen at elevated temperatures and that this newly established catalytic activity is intimately connected with the formation of substoichiometric ZrO_{2-x} centers,⁸ which have been shown in this work to molecularly bind H_2 .

4. CONCLUSION

The presented work on the reducibility of Y_2O_3 , YSZ, and ZrO_2 highlights the importance of their surface chemistry with respect to hydrogen adsorption and reactivity. As the most crucial parameter steering the adsorption and reactivity of hydrogen, the amount of surface OH-groups has been identified. As the reduction of the oxides has been observed to be basically restricted to surface or surface-near regions, this raises interesting questions how the chemical state and structure of the surface affect the technological application, e.g., the operation of solid-oxide fuel cells. A common feature of various oxides is the formation of molecular H_2 binding sites

after high-temperature reduction. However, the difference to more reducible oxides (e.g., Ga_2O_3 or In_2O_3) is that the formation of anionic vacancy sites with excitable donor electron states appears to be largely suppressed for the present three discussed oxides. In due course, the conductivity at high temperatures is independent of the oxide’s surface chemistry. It is also worth noting that on Ga_2O_3 and In_2O_3 , directed Ga–H bonds¹⁸ and In metal species¹⁹ have been formed upon reduction, respectively. For both cases, dissociatively activated hydrogen is a prerequisite. Furthermore, it will be of interest to extend these studies to the corresponding metal–oxide systems (especially Ni– and Cu– ZrO_2 systems relevant for methanol chemistry), as these systems represent the typical operating anodes in SOFC’s. Formation of special interfacial sites at the oxide–metal phase boundary or spillover of hydrogen activated on the metal surface might lead to more pronounced surface reduction of the oxides, which eventually may include also bulk reduction and/or more pronounced structural changes directly associated with metal–support interaction. By direct comparison of the experimental features of the pure oxides and the corresponding metal–oxide systems, the influence of the newly created phase boundary, suspected to represent the center of catalytic activity and selectivity, can in turn be elucidated. This would be especially worthwhile for Y_2O_3 and YSZ, where such experiments are clearly missing.

■ AUTHOR INFORMATION

Corresponding Author

*E-mail: simon.penner@uibk.ac.at. Tel.: 00435125075056. Fax: 00435125072925.

Author Contributions

[#]These two authors contributed equally to this work.

Notes

The authors declare no competing financial interest.

■ ACKNOWLEDGMENTS

We thank the FWF (Austrian Science Foundation) for financial support under the project F4503-N16.

■ REFERENCES

- (1) Jollet, F.; Noguera, C.; Thromat, N.; Gautier, M.; Duraud, J. P. Electronic Structure of Yttrium Oxide. *Phys. Rev. B* **1990**, *42*, 7587–7595.
- (2) Shen, Y.; Shao, S.; Yu, H.; Fan, Z.; He, H.; Shao, J. Influences of Oxygen Partial Pressure on Structure and Related Properties of ZrO_2 Thin Films Prepared by Electron Beam Evaporation Deposition. *Appl. Surf. Sci.* **2007**, *254*, 552–556.
- (3) Pailloux, F.; Imhoff, D.; Jublot, M.; Paumier, F.; Gaboriaud, R. J.; Jaouen, M. HRTEM and EELS Study of $\text{Y}_2\text{O}_3/\text{MgO}$ Thin Films. *Micron* **2006**, *37*, 420–425.
- (4) Oleshko, V. P.; Howe, J. M.; Shukla, S.; Seal, S. High-Resolution and Analytical TEM Investigation of Metastable-Tetragonal Phase Stabilization in Undoped Nanocrystalline Zirconia. *J. Nanosci. Nanotechnol.* **2004**, *4*, 867–875.
- (5) Gougos, T.; Chen, Z. Deposition of Yttrium Oxide Thin Films in Supercritical Carbon Dioxide. *Thin Solid Films* **2008**, *516*, 6197–6204.
- (6) Menzler, N. H.; Tietz, F.; Uhlenbruck, S.; Buchkremer, H. P.; Stöver, D. Materials and Manufacturing Technologies for Solid Oxide Fuel Cells. *J. Mater. Sci.* **2010**, *45*, 3109–3135.
- (7) Steiner, S. A., III; Baumann, T. F.; Bayer, C. B.; Blume, R.; Worsley, M. A.; MoberlyChan, W. J.; Shaw, E. L.; Schlögl, R.; Hart, A. J.; Wardle, B. L. Nanoscale Zirconia as Nonmetallic Catalyst for

- Graphitization of Carbon and Growth of Single- and Multiwall Carbon Nanotubes. *J. Am. Chem. Soc.* **2009**, *131*, 12144–12154.
- (8) Hoang, D. L.; Lieske, H. Effect of Hydrogen Treatments on ZrO₂ and Pt/ZrO₂ Catalysts. *Catal. Lett.* **1994**, *27*, 33–42.
- (9) Ponec, V. Cu and Pd, Two Catalysts for CH₃OH Synthesis: The Similarities and the Differences. *Surf. Sci.* **1992**, *272*, 111–117.
- (10) McTaggart, F. K. Reduction of Zirconium and Hafnium Oxides. *Nature* **1961**, *191*, 1192.
- (11) Friedrich, E.; Sittig, L. Herstellung und Eigenschaften von Nitriden. *Z. Anorg. Chem.* **1925**, *143*, 293.
- (12) Newbury, E.; Pring, J. N. The Reduction of Metallic Oxides with Hydrogen at High Pressures. *Proc. R. Soc. A* **1916**, *92*, 276.
- (13) Miller, T. M.; Grassian, V. H. A Mechanistic Study of Nitrous Oxide Adsorption and Decomposition on Zirconia. *Catal. Lett.* **1997**, *46*, 213–221.
- (14) Tomishige, K.; Sakahori, T.; Ikeda, Y.; Fujimoto, K. A Novel Method of Direct Synthesis of Dimethyl Carbonate from Methanol and Carbon Dioxide Catalyzed by Zirconia. *Catal. Lett.* **1999**, *58*, 225–229.
- (15) He, D.; Ding, Y.; Luo, H.; Li, C. Effects of Zirconia Phase On the Synthesis of Higher Alcohols Over Zirconia and Modified Zirconia. *J. Mol. Catal. A* **2004**, *208*, 267–271.
- (16) Pomfret, M. B.; Stoltz, C.; Varughese, B.; Walker, R. A. Structural and Compositional Characterization of Yttria-Stabilized Zirconia: Evidence of Surface-Stabilized, Low-Valence Metal Species. *Anal. Chem.* **2005**, *77*, 1791–1795.
- (17) Köck, E. M.; Kogler, M.; Bielz, T.; Klötzer, B.; Penner, S. In-Situ FT-IR Spectroscopic Study of CO₂ and CO Adsorption on Y₂O₃, ZrO₂, and Yttria-Stabilized ZrO₂. *J. Phys. Chem. C* **2013**, *117*, 17666–17673.
- (18) Jochum, W.; Penner, S.; Föttinger, K.; Rupprechter, G.; Klötzer, B. Hydrogen on Polycrystalline β -Ga₂O₃: Surface Chemisorption, Defect Formation, and Reactivity. *J. Catal.* **2008**, *256*, 268–277.
- (19) Bielz, T.; Lorenz, H.; Jochum, W.; Kaindl, R.; Klauser, F.; Klötzer, B.; Penner, S. Hydrogen on In₂O₃: Reducibility, Bonding, Defect Formation, and Reactivity. *J. Phys. Chem. C* **2010**, *114* (19), 9022–9029.
- (20) Grossmann, K.; Pavelko, R. G.; Barsan, N.; Weimar, U. Interplay of H₂, Water Vapor, and Oxygen at the Surface of SnO₂ Based Gas Sensors—An Operando Investigation Utilizing Deuterated Gases. *Sens. Actuators, B* **2012**, *166*, 787–793.
- (21) Hirose, F.; Kinoshita, Y.; Kanomata, K.; Momiyama, K.; Kubota, S.; Hirahara, K.; Kimura, Y.; Niwano, M. IR Study of Fundamental Chemical Reactions in Atomic Layer Deposition of HfO₂ with Tetrakis(ethylmethylamino)hafnium (TEMAH), Ozone, and Water Vapor. *Appl. Surf. Sci.* **2012**, *258*, 7726–7731.
- (22) Bianchi, D.; Gass, J. L.; Khalfallah, M.; Teichner, S. J. Intermediate Species on Zirconia Supported Methanol Aerogel Catalysts. 1. State of the Catalyst Surface Before and after the Adsorption of Hydrogen. *Appl. Catal., A* **1993**, *101* (2), 297–315.
- (23) Scherrer, B.; Schlupp, M.; Stender, D.; Martynczuk, J.; Grolig, J.; Ma, H.; Kocher, P.; Lippert, T.; Prestat, M.; Gauckler, L. On Proton Conductivity in Porous and Dense Yttria Stabilized Zirconia at Low Temperature. *Adv. Funct. Mater.* **2013**, *23*, 1957–1964.
- (24) Eder, D.; Kramer, R. Impedance Spectroscopy of Reduced Monoclinic Zirconia. *Phys. Chem. Chem. Phys.* **2006**, *8*, 4476–4483.
- (25) Hara, S.; Takano, S.; Miyama, M. Proton-Conducting Properties and Microstructure of Hydrated Tin Dioxide and Hydrated Zirconia. *J. Phys. Chem. B* **2004**, *108*, 5634–5639.
- (26) Singh, D.; Singh, R. Preparation of Eu⁺³ Doped Y₂O₃ and Core–Shell Y₂O₃: Eu–Y₂O₃ Nanoparticles: Photoluminescence Study. *Indian J. Eng. Mater. Sci.* **2009**, *16* (3), 175–177.
- (27) Zhang, Y.; Zhong, X. L.; Wang, J. B.; Song, H. J.; Ma, Y.; Zhou, Y. C. Dielectric and Switching Properties of a Metal–Ferroelectric (Bi_{3.15}Nd_{0.85}Ti₃O₁₂)–Insulator (Y₂O₃-Stabilized ZrO₂) Silicon Diode. *Appl. Phys. Lett.* **2010**, *97*, 103501.
- (28) Garcia, J. C.; Scolfaro, L. M. R.; Lino, A. T.; Freire, V. N.; Farias, G. A.; Silva, C. C.; Alves, H. W. L.; Rodrigues, S. C. P.; da Silva, E. F., Jr. Structural, Electronic, and Optical Properties of ZrO₂ from ab-Initio Calculations. *J. Appl. Phys.* **2006**, *100* (10), 104103.
- (29) Raz, S.; Sasaki, K.; Maier, J.; Riess, I. Characterization of Adsorbed Water Layers on Y₂O₃-Doped ZrO₂. *Solid State Ionics* **2001**, *143*, 181–204.